Struct Bond (2007) 125: 85–121
DOI 10.1007/430_2007_057

Published online: 12 May 2007

New Nitrogen-Rich High Explosives

Thomas M. Klapötke

Ludwig-Maximilian University Munich, Chair of Inorganic Chemistry,
Energetic Materials Research, Butenandtstrasse 5–13 (D), 81377 Munich, Germany
tmk@cup.uni-muenchen.de

Abstract The possibility of new high explosives based on nitrogen-rich tetrazole building blocks is discussed. The expected advantages include gaseous products, high heats of formation, high propulsive/expolosive power, high specific impulse, and high flame temperatures. In addition, these new explosives do not have the toxicity and environmental activity of currently used organo-nitro explosives. The synthesis and characteristics of a series of neutral tetrazole compounds are looked at as well as the neutral nitramine, dinitrobiuret.

Keywords Dinitrobiuret · High energy density materials · Nitrogen-rich · Polynitrogen · Tetrazole

Abbreviations

BTNA	Bistrinitroethylamine
DAT	1,5-Diaminotetrazole
DNB	Dinitrobiuret
EI	energetic ingredient
NTNAP	1-Nitrotetrazolato-2-nitro-2-azapropane
TNE	Trinitroethanol
MMTHT	1-Methyl-5-(1-methyl-2-(2,2,2-trinitroethyl)hydrazinyl)-1*H*-tetrazole
MTHTE	2-(5-(1-methyl-2-(2,2,2-trinitroethyl)hydrazinyl)-1*H*-tetrazol-1-yl)ethanol

1 Introduction

Environmental contamination by nitro compounds is associated principally with the explosives industry and military testing of explosives [1, 2]. The current widely used nitro-explosives are TNT (trinitrotoluene), RDX (Royal demolition explosive), and HMX (high melting explosive). The nitro-explosives per se as well as their environmental transformation products are toxic, with symptoms of exposure that include methemoglobinemia, kidney trouble, jaundice etc. For HMX, anaerobic or anoxic degradations have been described in many studies [3]. Explosives released into the environment at production and processing facilities, as well as through field use, may be toxic at relatively low concentrations to a number of ecological receptors [4]. Toxicity studies on soil organisms using endpoints such as microbial processes (potential nitrification activity, dehydrogenase activity, substrate-induced respiration, basal respiration), plant and seedling growth (*Lactuca sativa* and *Hordeum vulgare*), and earthworm (*Eisenia andrei*) growth and reproduction were carried out at contaminated sites. Results showed that HMX was the principal polynitro-organic contaminant measured in soils. Soils from the contaminated site showed decreased microbial processes and earthworm reproduction. However, plant growth was not significantly reduced [4]. Monocyclic nitramine explosives such as RDX and HMX are toxic to a number of ecological receptors, including earthworms [5–7]. The results of recent investigations suggest that organisms exposed to explosives at contaminated sites show hormetic growth enhancement at concentrations less than 25 $mg\,kg^{-1}$ and at higher concentrations through increased mortality [8]. Factors effecting leaching and transport, microbial degradation, phytotoxicity and plant uptake, and toxicity to invertebrates and vertebrates will determine the ultimate environmental fate and hazard potential [9]. It is clear that the release of explosives into the environment at production and processing facilities, as well as through field use, is a major point of concern.

Since the toxicity and environmental activity of organo-nitro explosives (TNT, RDX, HMX, see Fig. 1) are usually related to the presence of organo-nitro ($C-NO_2$), organo-nitroso ($C-NO$), or organo-nitrito ($C-ONO$) groups either in the explosive itself or its degradation products [10], the development of novel energetic ingredients (EIs) that lack the environmental hazards of the organo-nitro explosives is of great interest. The presently used EIs with the highest performance (RDX, HMX) as well as new, even more powerful EIs that are still under investigation (CL-20, hepta- and octacubane, see Fig. 1) all belong to the class of typical organic ring and cage molecules.

In this chapter we want to discuss the possibility of new high explosives that are neutral compounds and are based on nitrogen-rich tetrazole building blocks.

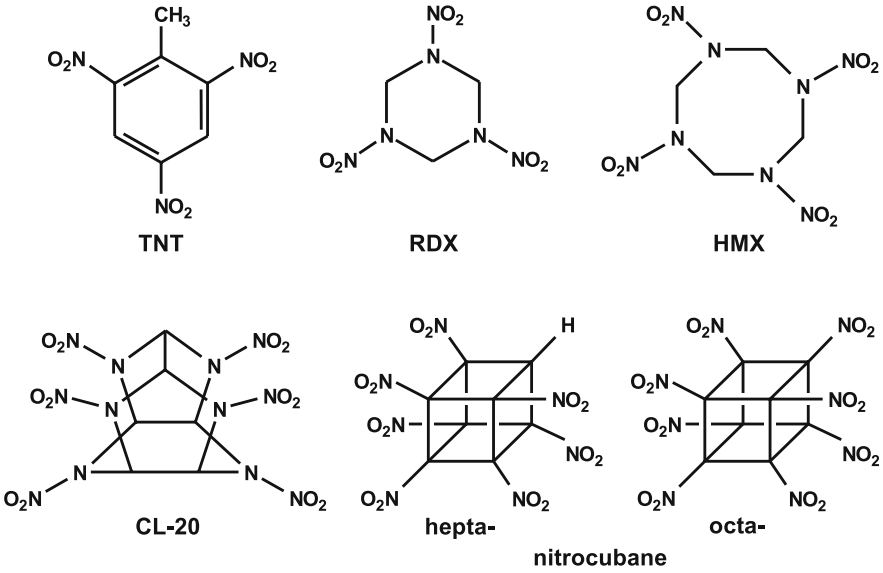

Fig. 1 Structures of TNT, RDX, HMX, CL-20, hepta-, and octa-cubane

The expected advantages of nitrogen-rich compounds include:

- Only gaseous products
- High heats of formation
- High propulsive/explosive power
- High specific impulse
- High flame temperatures

Also, recent modeling has shown that the presence of high concentrations of nitrogen species in the combustion products of propellants can reduce gun barrel erosion by promoting the formation of iron nitride rather than iron carbide on the interior surface of the barrel [11].

2 Strategies

Modern high-energy-density materials (HEDM) derive most of their energy from either:

1. Oxidation of the carbon backbone, as with traditional energetic materials
2. Ring or cage strain
3. Their very high positive heat of formation

Examples for the first class are traditional explosives such as TNT, RDX, HMX, and the recently reported 1,4-diformyl-2,3,5,6-tetranitropiperazine (Fig. 2). Modern nitro compounds such as CL-20 or the recently reported

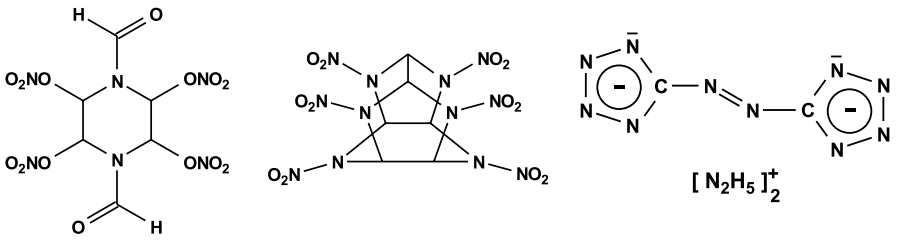

Fig. 2 Examples for EM that (i) show oxidation of the carbon backbone (*left*) [12], (ii) possess ring or cage strain (*center*) [13], or (iii) have very high positive heats of formation (*right*) [14]

hepta- and octanitrocubanes possess very high densities and enhance the energies utilizing substantial cage strain and therefore belong to the second class of explosives. Members of the third class of compounds are 5,5′-azotetrazolate salts, which show the desired remarkable insensitivity to electrostatic discharge, friction, and impact while having a very high (positive) heat of formation.

Nitrogen is unique amongst all other elements of the periodic table in so far that the bond energy per two-electron bond increases from a single over a double to a triple bond (Fig. 3). For carbon the situation is the opposite and one might expect acetylene (H – C ≡ C – H) to polymerize in an exothermic reaction whereas N_2 (N ≡ N) is more stable than any other polynitrogen species [15–18]. One may ask what the difference between formally sp-hybridized nitrogen in N_2 and sp-hybridized carbon in HCCH is. Indeed the bond situation is very similar and only an NBO analysis can help to explain the difference:

N ≡ N	σ(N – N)	64% s	36% p
	σ– LP(N)	34% s	66% p
H – C ≡ C – H	σ(C – C)	49% s	51% p
	σ(C – H)C	45% s	55% p
	H	100% s	

Whereas in acetylene the C – C σ bond is indeed essentially made up of sp-hybrid orbitals, in N_2 the σ bond orbitals have two-third s and only one-third p character and form therefore a much stronger bond than the carbon atoms do in HCCH.

With respect to all-nitrogen species (N_x), there are only a very few species known that have been isolated and characterized (Table 1).

Quite recently, researchers from the Max Plank Institute for Chemistry and the Geophysical Laboratory at the Carnegie Institution of Washington reported the polymerization of nitrogen in sodium azide [16–18]. With increasing pressure on sodium azide, the sample became completely opaque above

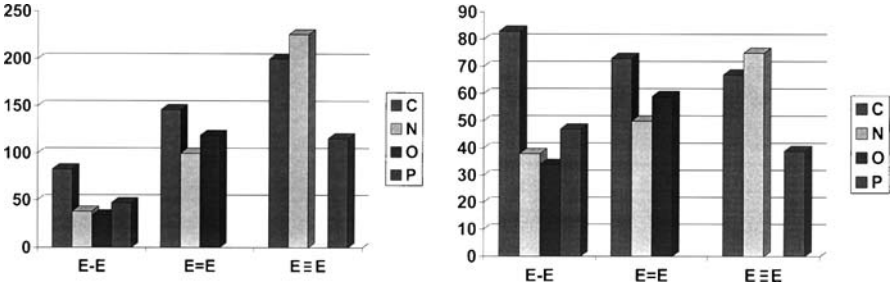

Fig. 3 Bond energies (in kcal mol^{-1}) for single, double and triple bonds (*left*) and per two-electron bond (*right*) [15]

Table 1 Isolated all-nitrogen species

All-nitrogen species	Name	Comment	Refs.
Neutral compounds			
N_2	Dinitrogen	Thermodynamic stable form of nitrogen, not energetic	[15]
cg-N_x	Cubic polynitrogen	Prepared from N_2 in diamond anvil cell at 200 K and 110 GPa; metastable only above 42 GPa	[16–18]
Ionic species			
N_3^-	Azide anion	Suitable energetic anion (or covalent azide group R-NNN)	[15]
N_5^+	Pentanitrogen cation	Metastable salts only with large counter anions ($Sb_2F_{11}^-$ etc.)	[19–21]
N_5^-	Pentanitrogen anion	Only detected in the gas phase (mass spectrometry)	[22, 23]

120 GPa, evidencing completion of the transformation to a non-molecular nitrogen state with amorphous-like structure that crystallized after laser heating to 3300 K. This change was interpreted in terms of a transformation of azide ions to larger nitrogen clusters and subsequent formation of a polynitrogen network. The polymeric form was preserved on decompression in the diamond anvil cell, but transformed back to the starting azide form under ambient conditions.

In an another publication [17], Eremets et al. reported a single-bonded cubic form of nitrogen. This material was synthesized directly from molecular nitrogen at temperatures above 2000 K and pressures above 110 GPa, again in a laser-heated diamond-cell. From X-ray and Raman scattering the substance was identified as the long-sought-after polymeric nitrogen with the

theoretically predicted cubic gauche structure (cg-N). In this compound, each nitrogen atom is connected to three neighbors by three single covalent bonds (Fig. 4). This is a new member of a class of single-bonded nitrogen materials with unique properties such as an energy capacity more than five times that of most powerful non-nuclear energetic materials.

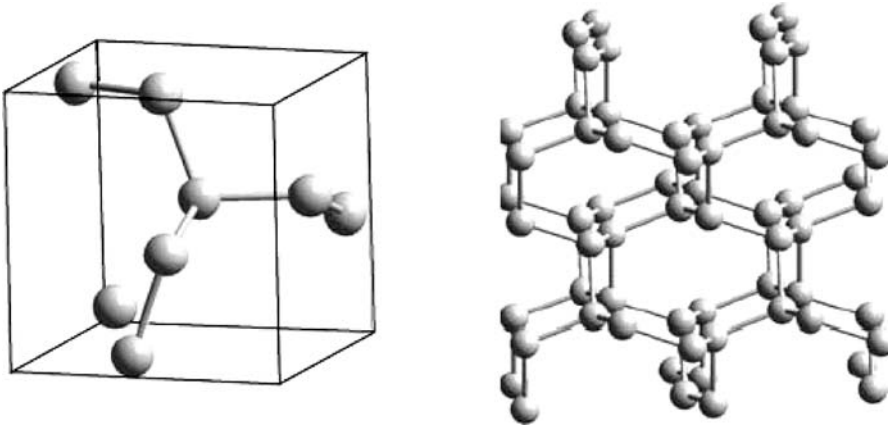

Fig. 4 cg-N structure. Each N atom is connected to three neighbors by three single covalent bonds. The primitive cell is shown on the *left*, and an extended structure of the polymeric N is shown on the *right*

The authors confirmed calculations that predicted that the cg-structure is the most energetically favorable. Their findings confirm the existence of a new allotrope of nitrogen where atoms are connected with single covalent bonds (cf. Fig. 4). The predicted wide band-gap of 8.1 eV (or 3.75 eV at 240 GPa) correlates well with the observed colorless transparent phase. Although theory also predicts that the cg-N could be metastable at atmospheric pressures, Eremets et al. found that at room temperature cg-N is metastable at pressures above 42 GPa. At this pressure, it transforms to a molecular phase under weak laser illumination. If cg-N is not metastable at ambient pressure, the authors hope it can be stabilized in compounds with other elements or by introducing impurities.

Only further experiments can show whether this new form of polynitrogen may ever be suitable for use as a high energy density material (HEDM), due to (i) its very high expected specific impulse (for propulsion) or, less likely, (ii) expected high explosive power (for use as a secondary explosive or high explosive). Whether polynitrogen finds application or not, the authors ought to be congratulated on their outstanding and break-through discovery.

In addition, there are numerous polynitrogen species that have been computed in the gas phase (Fig. 5) [24–30], however, none of these compounds has yet been prepared in the laboratory, not even on a milligram scale.

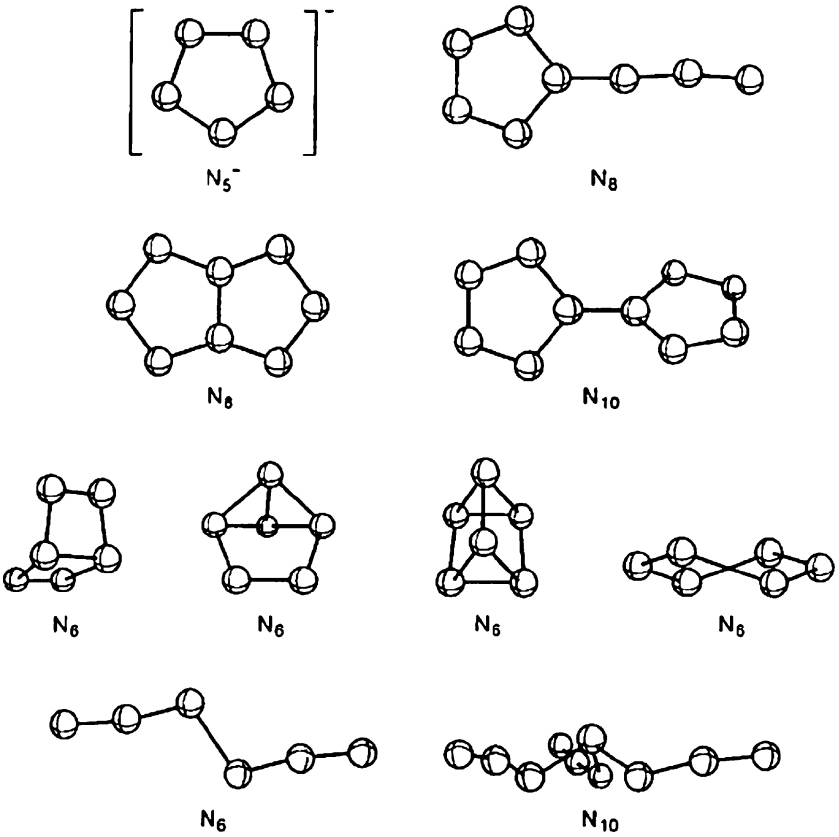

Fig. 5 Structure of N_5^- and some computationally known (but not yet synthesized) neutral polynitrogen species [24–30]

In the opinion of the author of this chapter high-nitrogen compounds (in contrast to all-nitrogen compounds) clearly have great potential as new energetic materials. Whereas high-nitrogen compounds without additional oxidizing groups may be good candidates for use as propellant charges for high explosives, the combination of high-nitrogen compounds with strongly oxidizing nitro, nitrato, nitramino, or nitrimino groups should be advantageous in delivering the explosive energy required (Fig. 6).

In order to stabilize nitrogen-rich molecules, π aromatic delocalization may be used. In this context five-membered heterocycles with three N atoms – triazoles –, four N atoms – tetrazoles –, and five N atoms – pentazoles – play an important role (Fig. 7). While triazoles often do not possess enough intrinsic energy to be suitable candidates for high explosives, pentazole derivatives are usually either far too sensitive and unstable for any application or need to be kinetically stabilized by bulky groups, which reduce the nitrogen con-

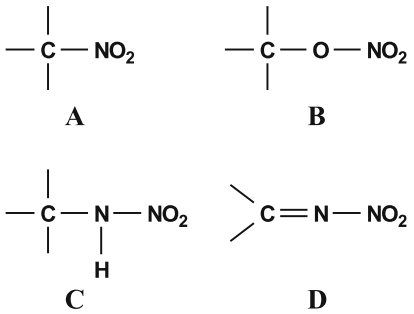

Fig. 6 Nitro (*A*), nitrato (*B*), nitramino (*C*), and nitrimino (*D*) groups

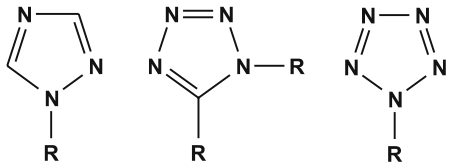

Fig. 7 Neutral triazole, tetrazole, and pentazole

tent substantially. Therefore, tetrazole compounds seem to be a good choice for combining high-nitrogen content with reasonable kinetic stability.

Energetic salts are important systems for the development of high energy density materials since salts are intrinsically non-volatile, are typically thermally stable under normal conditions, and are more dense [31, 32]. However, due to the fact that salts tend to have undesirable octanol/water partition coefficients and may therefore find their way into the groundwater, in this review we therefore want to focus on neutral species.

3
Neutral Tetrazole Compounds

3.1
1,5-Diaminotetrazole (DAT)

Because of the difficult accessibility of 1,5-diaminotetrazole (DAT, Fig. 8), only few synthetic methods for its preparation have been described in the literature. This compound, as all aminotetrazoles, has the highest content of nitrogen among organic substances (about 84%) and due to the aromaticity, it exhibits a relatively high thermal stability.

In addition, DAT presents a high energy of formation; for this reason it can be used as a valuable intermediate in the preparation of high-energy-density materials [33–35].

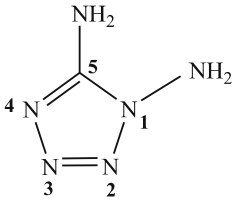

Fig. 8 Structure of 1,5-DAT

A milestone in the synthesis of DAT was described by Raap [36] who reacted the sodium salt of 5-aminotetrazole with hydroxylamine-*O*-sulfonic acid and obtained a mixture of 1,5-diaminotetrazole (1,5-DAT) and 2,5-diaminotetrazole (2,5-DAT), where the first constitutes 8.5% of the reaction yield (Fig. 9).

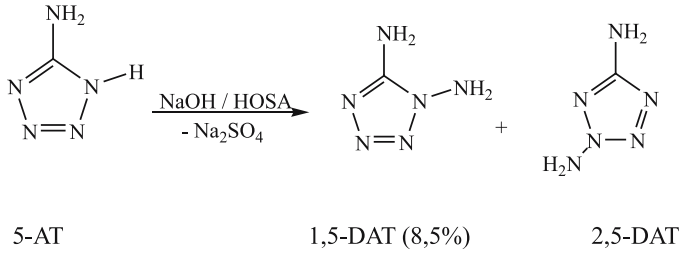

Fig. 9 Synthesis of 1,5-DAT and 2,5-DAT according to Raap [36]

Before Raap, Gaponik et al. [37] improved the synthesis reported by Stolle et al. [38]. By reacting thiosemicarbazide with lead oxide and sodium azide in a CO_2 atmosphere, a carbodiimide intermediate is formed and reacts in situ with HN_3 to lead to 1,5-DAT (Fig. 10). Unfortunately, this reaction leads to large amounts of lead azide as the side-product, which makes this synthesis problematic for an industrial scale.

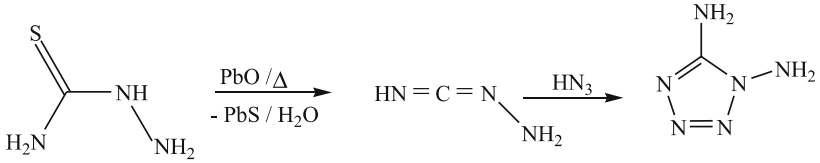

Fig. 10 Synthesis of 1,5-DAT using PbO [37, 38]

The most recent approach to the synthesis of DAT was made at LMU Munich [39, 40] and eliminates the formation of highly explosive lead azide

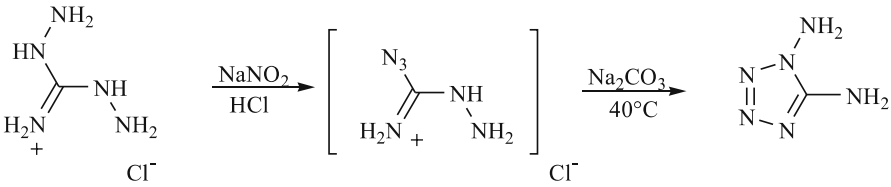

Fig. 11 Improved synthesis of 1,5-DAT without using PbO [39–41]

and produces a substantially greater yield. After diazotation of diaminoguanodinium chloride, the reaction mixture is brought to pH 8 to deprotonate the intermediate formed, which cyclizes yielding 1,5-DAT in 58% yield (Fig. 11). Nevertheless, the synthesis conditions must be perfectly controlled because the reaction of nitrous acid with aminoguanidinium is strongly dependent on the pH value as well as on the amounts of reactants, otherwise it might lead to the azide derivative, which is a very explosive by-product [41].

3.2
1-Nitrotetrazolato-2-nitro-2-azapropane (NTNAP)

The reaction of 1-chloro-2-nitro-2-azapropane with silver nitrotetrazolate yielded 1-nitrotetrazolato-2-nitro-2-azapropane (NTNAP) as a white solid in over 90% yield (Fig. 12) [42].

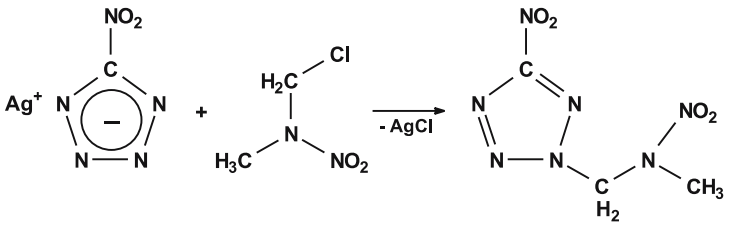

Fig. 12 Synthesis of NTNAP

The molecular structures of NTNAP in the crystalline state was determined by low-temperature X-ray crystallography (Fig. 13). The aromatic tetrazolium ring is, as expected, planar with the following torsion angles: C1 – N1 – N2 – N3 0.2(2)°, N2 – N1 – C1 – N4 – 0.4(2)°, N1 – N2 – N3 – N4 0.0(2)°. The crystalline density was determined to be 1.735 g cm^{-3}.

NTNAP was fully characterized by IR and Raman spectroscopy and multinuclear NMR spectroscopy (^{1}H, ^{13}C, ^{14}N). The nitrotetrazolium compound shows a rather complex ^{14}N NMR spectrum, however, the two nitro (– NO_2) resonances are well resolved at – 26.2 and – 28.7 ppm. In the ^{13}C NMR spec-

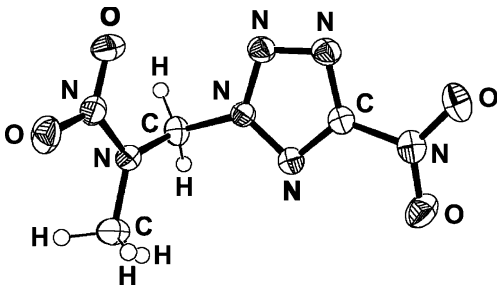

Fig. 13 Molecular structure of NTNAP in the crystalline state. Displacement ellipsoids are shown at the 50% probability level

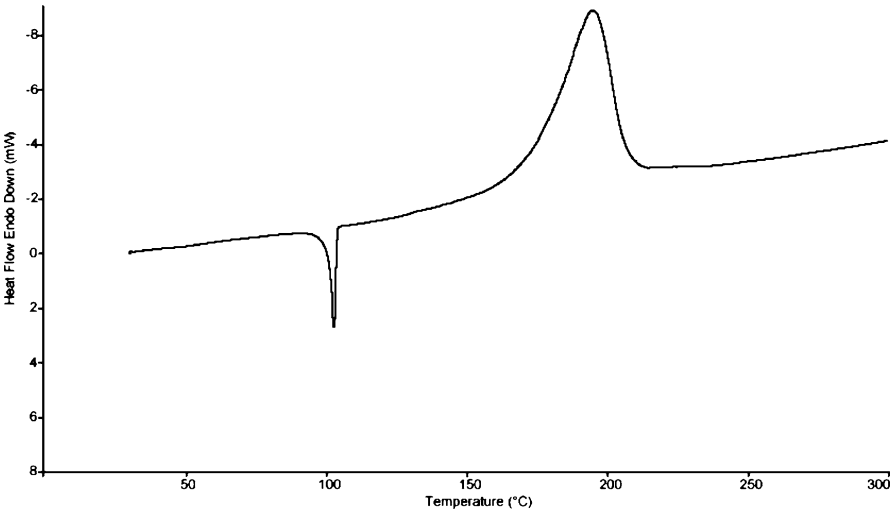

Fig. 14 DSC plot of NTNAP, heating rate 2 °C min^{-1}

trum the methyl (– CH_3, 3.55 ppm) and methylene (– CH_2 –, 6.85 ppm) protons show singlet resonances clearly shifted, as expected, to low field.

The DSC plot of NTNAP was recorded with a heating rate of 2 °C min^{-1} (Fig. 14). The covalent compound is thermally reasonably stable, melts without decomposition at 100 °C, and shows decomposition with an onset of about 180 °C. Therefore, the compound possesses properties that may make it suitable for melt-casting processes.

The sensitivity and detonation parameters of NTNAP are summarized in Table 2.

Table 2 Energetic properties of NTNAP

	NTNAP
Appearance	White powder
Stability	Hydrolytically stable
Deflagration	Explodes when thrown in a flame
Oxygen balance [%]	– 35.5
Impact sensitivity [J] [18, 19]	6
Friction sensitivity [N]	60

3.3 *N*-Trinitroethyl Derivatives of Nitrogen Containing Compounds

Although compounds carrying the *N*-trinitroethyl fragment have been reported, relevant data were published mainly in the patent literature, often without giving information about synthetic procedures or specifying the physicochemical characteristics of the compounds obtained. In the course of investigations into high energy density materials (HEDM) at LMU Munich, we recently focused our attention on new derivatives of energetic materials that combine both the advantages of the tetrazole, as well as the trinitroethyl, moiety. The tetrazole unit with its high nitrogen content together with its endothermic character is remarkably thermodynamically stable and the trinitroethyl fragment contributes to a positive oxygen balance.

Trinitroethanol (TNE) and bistrinitroethylamine (BTNA) can easily be synthesized according to the literature [43, 44]. The best synthetic approach for the synthesis of 1-methyl-5-(1-methyl-2-(2,2,2-trinitroethyl)hydrazinyl)-1*H*-tetrazole (MMTHT) and 2-(5-(1-methyl-2-(2,2,2-trinitroethyl)hydrazinyl)-1*H*-tetrazol-1-yl)ethanol (MTHTE) utilizes a condensation of the starting amino derivative with 2,2,2-trinitroethanole (Fig. 15) [45].

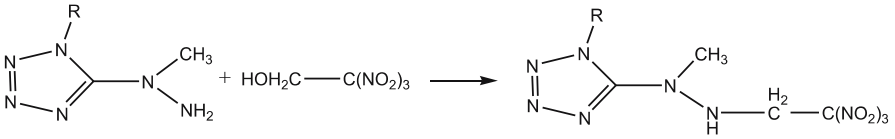

R = CH_3, CH_2CH_2OH

Fig. 15 Synthesis of MMTHT and MTHTE

All compounds were characterized using vibrational spectroscopy. In addition, TNE, MMTHT, and MTHTE were characterized using ^{1}H, ^{13}C, and

Table 3 Properties of MMTHT

Sum formula	$C_5H_9N_9O_6$
Formula weight [g mol^{-1}]	291.21
TMD [g cm^{-3}]	1.63
$T_{decomposition,\ onset}$ (DSC, 2 K min^{-1}) [°C]	82.5
$-\Delta_c U$ [cal g^{-1}]	2936
Impact sensitivity [J]	> 30
Friction sensitivity [N]	108 (visible flame)
Oxygen balance [%]	– 46.7
$-\Delta_f U$ [kJ kg^{-1}]	+ 1889
Q_V [kJ kg^{-1}]	– 6368
T_{ex} [K]	4404
P [kbar]	277
D [m s^{-1}]	8307
V_0 [L kg^{-1}]	783

Table 4 Selected structural data of TNE, BTNA, MMTHT, and MTHTE

Compound	TNE	BTNA	MMTHT	MTHTE
Formula	$C_2H_3N_3O_7$	$C_4H_5N_7O_{12}$	$C_5H_9N_9O_6$	$C_6H_{11}N_9O_7$
Formula weight [g mol^{-1}]	181.07	343.12	291.21	321.208
Temperature [K]	200	200	100	100
Crystal system	Monoclinic	Orthorhombic	Triclinic	Monoclinic
Space group	$P2_1/c$ (no. 14)	P bca (no. 61)	P-1	$P2_1/n$ (no. 14)
a [Å]	6.1218(4)	12.8996(6)	7.2651(13)	13.0419(4)
b [Å]	18.8120(12)	11.7753(5)	7.5773(16)	7.3020(2)
c [Å]	11.7391(8)	16.1577(7)	11.695(7)	14.8002(5)
α [°]	90	90	102.89(3)	90
β [°]	104.997(4)	90	103.82(3)	112.118(4)
γ [°]	90	90	99.387(17)	90
Volume [Å^3]	1305.87(15)	2454.30(19)	593.3(4)	1305.73(7)
Z	8	8	2	4
Absorption coefficient [mm^{-1}]	0.191	0.188	0.146	0.147
Density exptl. [g cm^{-3}]	1.842	1.857	1.630	1.634
$F(000)$	736	1392	300	664
2θ [°]	51.0	51.5	52.0	54.0
Reflections collected	12556	22836	5227	9034
Reflections unique	2424	2330	2308	2831
R_{int}	0.0631	0.0494	0.0225	0.0237
Parameters	237	228	217	243
GOOF	1.223	1.294	0.979	1.061
R_1/wR_2 [I > 2σ(I)]	0.0651/0.1048	0.0802/0.1766	0.0300/0.0730	0.0297/0.0740
R_1/wR_2 (all data)	0.0825/0.1135	0.0831/0.1787	0.0432/0.0772	0.0438/0.0806

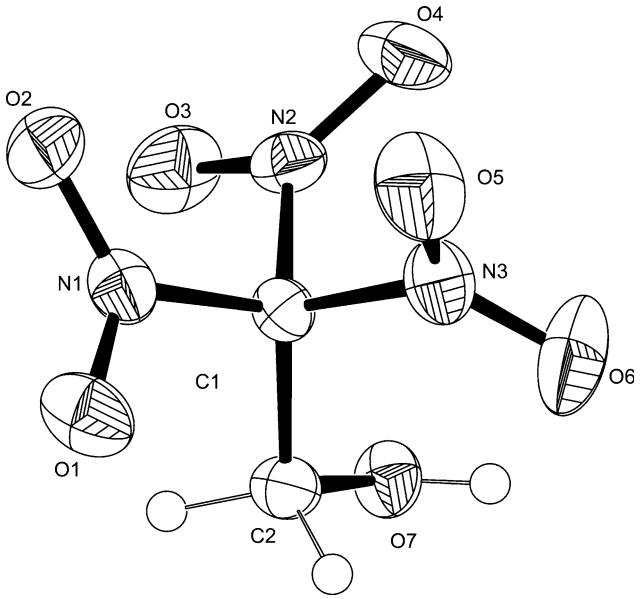

Fig. 16 ORTEP representation of the molecular structure of TNE in the crystalline state. The thermal ellipsoids are shown at the 50% probability level

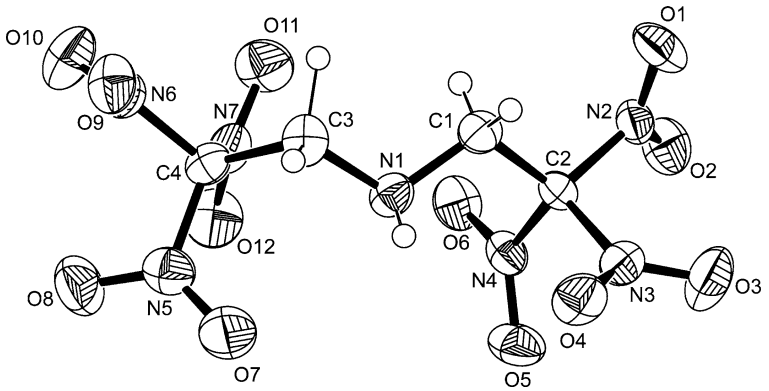

Fig. 17 ORTEP representation of the molecular structure of BTNA in the crystalline state. The thermal ellipsoids are shown at the 50% probability level

$^{14/15}$N NMR spectroscopy, mass spectrometry, and elemental analysis. Their impact, friction, and electrostatic sensitivity data were measured in order to establish safe handling procedures for these compounds (Table 3). Furthermore, all compounds have been structurally fully characterized using single crystal X-ray diffraction methods (Table 4, Figs. 16–19).

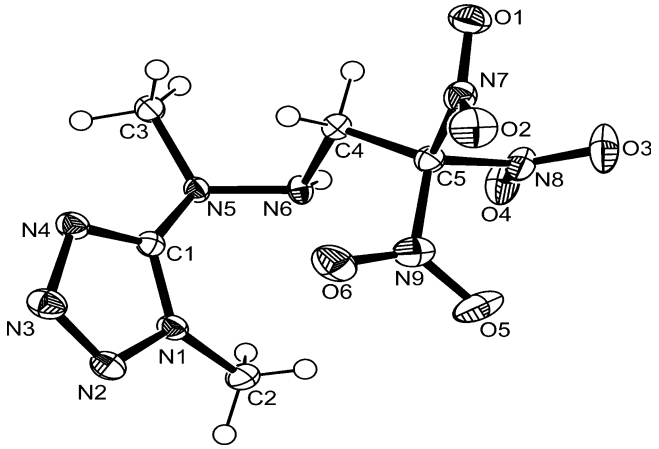

Fig. 18 ORTEP representation of the molecular structure of MMTHT in the crystalline state. The thermal ellipsoids are shown at the 50% probability level

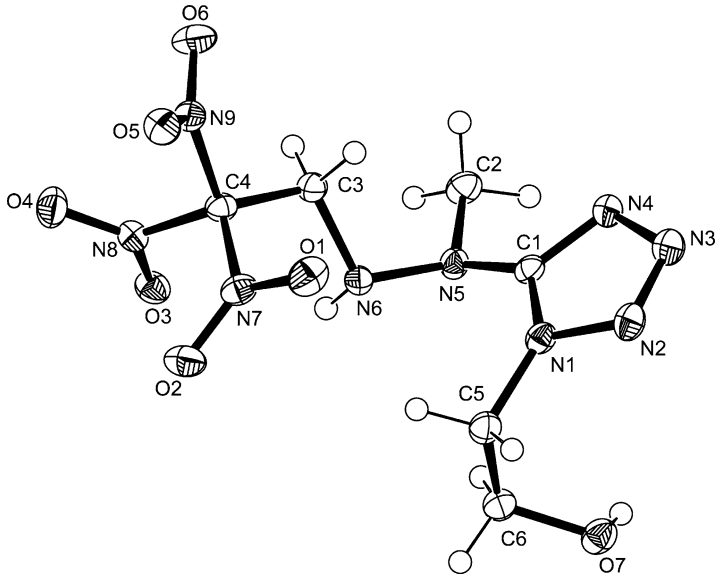

Fig. 19 ORTEP representation of the molecular structure of MMTHT in the crystalline state. The thermal ellipsoids are shown at the 50% probability level

3.4 Nitrated Aminotetrazoles

The combination of a tetrazole ring with energetic groups containing oxygen such as nitro groups ($R-NO_2$) [46], nitrate esters ($R-O-NO_2$) [47],

or nitramines (R_2N-NO_2) [48] is of particular interest. Energetic materials based on tetrazoles show the desirable properties of high nitrogen contents on the one hand, and astonishing kinetic and thermal stabilities due to aromaticity on the other. Compounds with a high nitrogen contend are potential candidates for replacing common secondary explosives like RDX [49] (hexahydro-1,3,5-trinitro-*S*-triazine) and HMX [50] (octahydro-1,3,5,7-tetranitro-1,3,5,7-tetrazine), or in high-tech propellants when combined with a suitable oxidizer [51]. Nitroaminotetrazoles are of special interest because they combine both the oxidizer and the energetic nitrogen-rich backbone in one molecule.

The nomenclature of nitroaminotetrazoles (also referred to as nitramino- or nitriminotetrazoles) is usually inconsistent in literature [52] as a result of incomplete characterization of the previously reported compounds. Therefore, a complete characterization of three well-known nitroaminotetrazoles is given in this chapter (see also [53]). The crystal structures show the first examples of neutral 5-aminotetrazoles that have been nitrated at the primary NH_2 group. For 5-nitroaminotetrazole only the cell parameters have been previously published [54], while several examples of 5-methylnitraminotetrazoles have been structurally characterized and reported in the literature [55]. On the basis of the crystal structures obtained, the nitration product of 5-aminotetrazole (**1**) is now referred to as 5-nitriminotetrazole (**2**).

Nitriminotetrazoles and the corresponding metal nitramino-tetrazolates salts [56–58] have been known for a long time since they are cheap and easy to manufacture via various routes. However there are two main methods. The first synthesis uses protonation of 5-aminotetrazole (**1**) [59] using warm concentrated HNO_3 to form 5-aminotetrazole nitrate, followed by dehydration with concentrated sulfuric acid [60, 61] to form **2**. Another synthetic route is based on the cyclization of nitroguanylazide [62–64] (also known as nitroazidoformamidine). A further method is the N-nitration of aminotetrazoles using tetranitromethane [65, 66].

The investigated compounds **2**, **5**, and **6** are prepared starting from the corresponding 5-amino-1*H*-tetrazoles. 5-Aminotetrazole (**1**, 5-AT), first described by Thiele in 1892 [67], can be easily alkylated forming the methyl derivatives [68, 69]. The investigated and probably simplest way for preparing 5-nitriminotetrazole is the treatment of 5-aminotetrazole with fuming HNO_3 (Fig. 20).

The single crystal X-ray diffraction data were collected using an Oxford Xcalibur3 diffractometer with a Spellman generator (voltage 50 kV, current 40 mA) and a KappaCCD detector. The data collections were undertaken using the CrysAlis CCD software [70] and the data reductions were performed with the CrysAlis RED software [71]. The structures were solved with SIR-92 [72] and refined with SHELXL-97 [73] and finally checked using PLATON [74]. In all structures the hydrogen atoms were found and refined. The absorptions of **5** and **6** were corrected using the SCALE3 ABSPACK multiscan

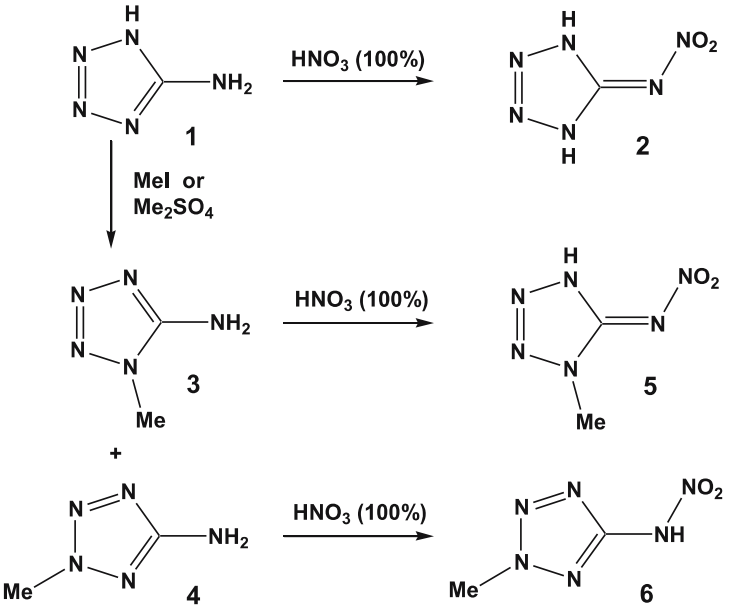

Fig. 20 The reaction of 5-aminotetrazole (**1**), 1-methyl-5-aminotetrazole (**3**), and 2-methyl-5-aminotetrazole (**4**) with 100% HNO_3

method [75]. In the chiral space group $P2_12_12_1$ the Friedel pairs were merged. Selected data from the X-ray data collection and refinements are given in Table 5. Further information regarding the crystal structure determinations has been deposited with the Cambridge Crystallographic Data Centre [76] as supplementary publication numbers 635164 (**2**), 635163 (**5**), and 635160 (**6**).

Compound **2** was characterized as a dibasic acid with pK_a values of 2.5 and 6.1 [60]. Previously it was not possible to locate the hydrogen atoms and it was assumed that the more acid hydrogen is located at the nitramino group [77]. However, using single crystal diffraction both hydrogen atoms were located on the tetrazole ring at nitrogen atoms N1 and N4. The ^{15}N NMR spectra shows only four signals, which suggests the same connectivity present in solution. DFT calculations show that this isomer is the one calculated lowest in energy even in the gas phase. The molecular unit can be seen in Fig. 21.

The geometry of the tetrazole ring in **2** can be compared with that of 5-aminotetrazole monohydrate (5-AT) [78]. The bond lengths in **2** are about 1.0 Å shorter than in 5-AT, with the shortest distance in **2** between the atoms N2 and N3 with 1.278(1) Å and the longest between N1 and N2 with 1.358(1) Å. The C1 – N5 bond length is 1.341(1) Å, which is closer to a C = N double bond (1.28 Å) than a C – N single bond (1.46 Å), whereas the nitramine bond N5 – N6 is considerably longer (1.363(1) Å). The angles in **2** differ from those in 5-AT. The N4 – C1 – N1 angle in **2** (103.9(1)°) is smaller than in 5-AT (107.9(1)°), which can be explained using the VSEPR

Table 5 Crystallographic data for compounds **2**, **5**, and **6**

	2	**5**	**6**
Formula	$CH_2N_6O_2$	$C_2H_4N_6O_2$	$C_2H_4N_6O_2$
Form. weight [g mol^{-1}]	130.09	144.11	144.11
Crystal system	Monoclinic	Orthorhombic	Monoclinic
Space Group	$P2_1/c$ (14)	$P2_12_12_1$ (19)	$P2_1/c$ (14)
Color/habit	Colorless cuboids	Colorless rods	Colorless blocks
Size [mm]	0.18 × 0.13 × 0.08	0.19 × 0.16 × 0.08	0.24 × 0.18 × 0.15
a [Å]	9.4010(3)	6.6140(1)	9.5278(9)
b [Å]	5.4918(1)	8.5672(2)	7.7308(7)
c [Å]	9.3150(3)	19.2473(4)	8.4598(9)
α [°]	90.0	90.0	90.0
β [°]	105.762(3)	90.0	112.875(9)
γ [°]	90.0	90.0	90.0
V [Å^3]	462.84(2)	1090.62(4)	574.1(1)
Z	4	8	4
ρ_{calc} [g cm^{-3}]	1.867	1.755	1.667
μ [mm^{-1}]	0.169	0.153	0.145
$F(000)$	264	592	296
$\lambda_{MoK\alpha}$ [Å]	0.71073	0.71073	0.71073
T [K]	100	100	200
θ min, max [°]	4.3, 32.1	3.7, 32.1	4.6, 26.0
Dataset	– 13 : 13; – 8 : 8; – 13 : 13	– 9 : 9; – 12 : 12; – 28 : 27	– 11 : 11; – 9 : 9; – 10 : 10
Reflections collected	6375	15881	5625
Independent reflections	1537	2104	1128
R_{int}	0.037	0.034	0.034
Observed reflections	1050	1616	1087
No. parameters	90	213	107
R_1 (obs)	0.0343	0.0297	0.0440
wR_2 (all data)	0.0960	0.0696	0.0950
GooF	1.00	0.99	1.21
Weighting scheme	0.05710	0.04220	0.03930 0.16880
Resd. Density [e/ Å^3]	– 0.23, 0.31	– 0.32, 0.21	– 0.22, 0.17
Device type	Oxford Xcalibur3 CCD	Oxford Xcalibur3 CCD	Oxford Xcalibur3 CCD
Solution	SIR-92	SIR-92	SIR-92
Refinement	SHELXL-97	SHELXL-97	SHELXL-97
Absorption correction	None	Multiscan	Multiscan
CCDC	635164	635163	635160

model [79] in which a double bond requires more space. A condition of the 6π-Hückel-aromaticity is a planar ring system, which can be seen at the torsion angle between N1 – N2 – N3 – N4 of 0.5(1)°. The nitramine

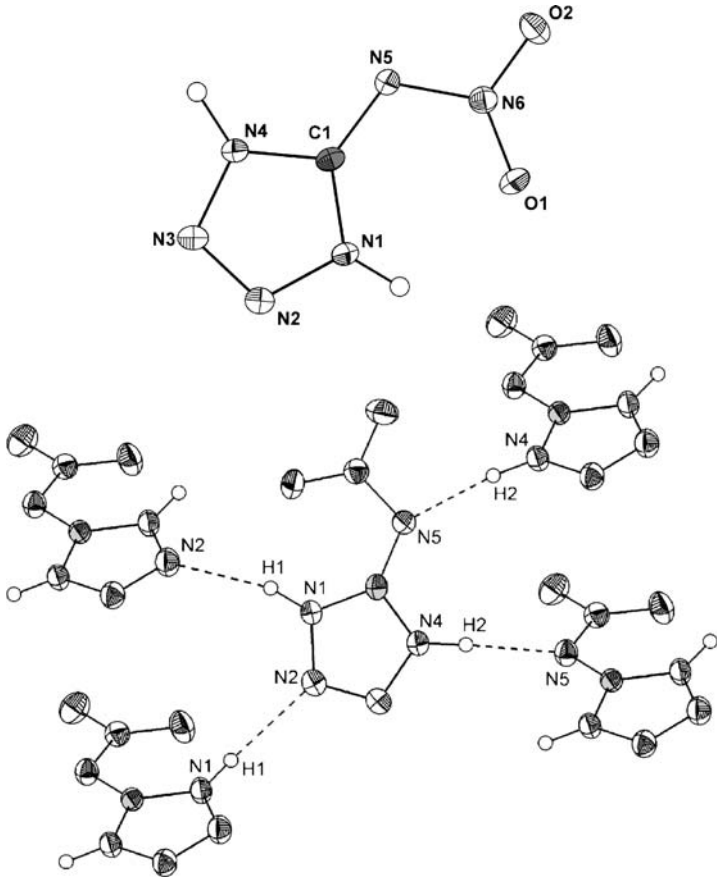

Fig. 21 *Left*: View of the molecular structure of **2** with thermal ellipsoid drawn at the 50% probability level. Hydrogen atoms are shown as small spheres of arbitrary radii. *Right*: H-bonding in **2** (N1 – H1 – N2^{i}: D – H 0.89(2) Å, H – A 2.11(2) Å, D – A 2.948(1) Å, D – H – A 156 (1)°; N4 – H4 – N5^{ii}: 0.98(2) Å, 1.83(2) Å, 2.850(2) Å, 175 (2)°; N4 – H4 – O2^{ii}: 0.98(2) Å, 2.48(2) Å, 3.146(1) Å, 125 (1)°; N4 – H4 – N6^{ii}: 0.98(2) Å, 2.58(2) Å, 3.4748(14) Å, 153 (1)°; ((i) 1 – *x*, 0.5 + *y*, 1.5 – *z* (ii) 2 – *x*, – 0.5 + *y*, 1.5 – *z*))

group also shows only slight derivations from the planarity (torsion angle C1 – N5 – N5 – O1 1.8(1)°), and is stabilized via a intramolecular hydrogen bond between N1 – H1 – O1. Bond lengths for the non-hydrogen atoms in **2** are given in Table 6. Each 5-nitriminotetrazole molecule participates in two strong intermolecular hydrogen bonds, as is illustrated in Fig. 21. The strong hydrogen bonds appear to be the most important reason for the high density of 1.867 g cm^{-3}.

Accordingly, the densities of **5** and **6** decrease because of the presence of the methyl groups. The molecular unit of **5** (Fig. 22) shows a similar con-

Table 6 Bond lengths of **2**, **5**, and **6**

Atoms	Bond length d(1–2) [Å]		
	2	**5**	**6**
O2 – N6	1.234(1)	1.234(2)	1.224(2)
O1 – N6	1.237(1)	1.266(2)	1.217(2)
N1 – N2	1.358(1)	1.355(2)	1.327(2)
N1 – C1	1.341(1)	1.345(2)	1.325(2)
N4 – C1	1.336(1)	1.338(2)	1.339(2)
N4 – N3	1.352(1)	1.364(2)	1.321(2)
N2 – N3	1.278(1)	1.284(2)	1.318(2)
N5 – N6	1.363(1)	1.338(2)	1.379(2)
N5 – C1	1.341(1)	1.346(2)	1.397(2)
N1(2) – C2		1.455(2)	1.459(2)

nectivity to that of **2**, whereby the N1 – H group in **2** has been substituted by a methyl group at atom N1. Again, in **5** the nitro group is tilted sideways where the hydrogen atom is located, forming an intramolecular hydrogen bond. In **5**, the nitrimine unit is also found to lie in the plane of the tetrazole ring (torsion angle O1 – N6 – N5 – C1 of 4.3(2)°), whereby the tetrazole ring in **5** shows comparable bond lengths with those observed in **2**. The most significant difference is the nitramine bond between N5 and N6, which is shorter in compound **5** (d (N5 – N6) = 1.338(2) Å). Finally, there is no significant differences for the angles observed in compounds **2** and **5**. The structure observed for **5** in the crystalline state is again influenced by several strong intermolecular hydrogen bonds, which are illustrated in Fig. 22.

The structure of **6** is considerably different to the structures of **2** and **5** discussed previously. The methyl group at the nitrogen atom N2 directs the remaining proton to the nitrogen atom N5, building a nitraminotetrazole (Fig. 23). In **6**, the C1 – N5 bond length is crucially longer with a distance of 1.397(2) Å and the nitramine unit does not lie in the plane of the tetrazole ring, as is clearly shown by the C1 – N5 – N6 – O1 torsion angle of – 19.2(2)°. The N6 – N5 – C1 angle (117.9(1)°) is larger than is observed in **2** and **5**, and the N5 – N6 nitramine bond of 1.379(2) Å is the longest in this series of compounds and can be seen as contributing to the low density of 1.667 g cm^{-3}, which is the lowest among the three structures discussed in this work. Further reasons for the lower observed density of **6** are the absence of strong intramolecular hydrogen bonds and the presence of only two moderately strong hydrogen bonds, as illustrated in Fig. 23. Relevant structural parameters are listed in Tables 6 and 7.

Vibrational spectroscopy is a suitable method for identifying nitraminotetrazoles. The IR and Raman (Fig. 24) spectra of compounds **2**, **5**, and **6** show

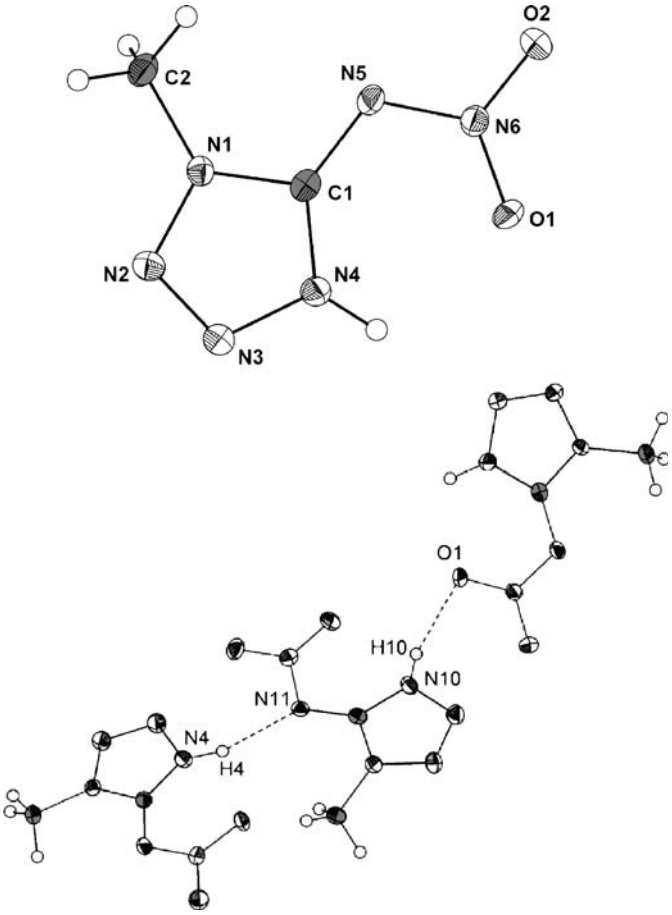

Fig. 22 *Left*: View of the molecular structure of **5**, representing the half of the asymmetric unit. Thermal ellipsoid are drawn at the 50% probability level and hydrogen atoms are shown as small spheres of arbitrary radii. *Right*: H-bonding in **5** (N4 – H4 – N11^{i}: D – H 0.93(2) Å, H – A 1.96(2) Å, D – A 2.848(2) Å, D – H – A 158 (2)°; N4 – H4 – O4: 0.93(19) Å, 2.59(2) Å, 3.098(2) Å, 115.3(15)°; N10 – H10 – O1^{i}: 0.80(2) Å, 2.10(2) Å, 2.874(2) Å, 163 (2)°; ((i) – *x*, 0.5 + *y*, 0.5 – *z*))

the vibrations expected from comparison with similar compounds in the literature [80, 81]. The N – NO_2 groups result in the strong absorptions in the 1280–1300 ($\nu_{sym}(NO_2)$) and 1560–1620 ($\nu_{asym}(NO_2)$) cm^{-1} regions as well as to a weak band at 945–970 (ν(N – N)) cm^{-1} [82]. The IR and Raman spectra of compounds **2**, **5**, and **6** show further characteristic absorption bands in the regions listed below: 3250–3100 cm^{-1} [ν(N – H)], 3000–2850 [ν(C – H) **5**, **6**], 1680–1550 [ν(N – H)], 1550–1350 [ν, tetrazole ring, $\nu_{as}(CH_3)$], ~ 1380 [$\nu(CH_3)$], 1350–700 [ν(N1 – C1 – N4), ν(N – N), ν(N – H), ν, tetrazole ring], < 700 [$\nu\delta_{oop}$(N – H)].

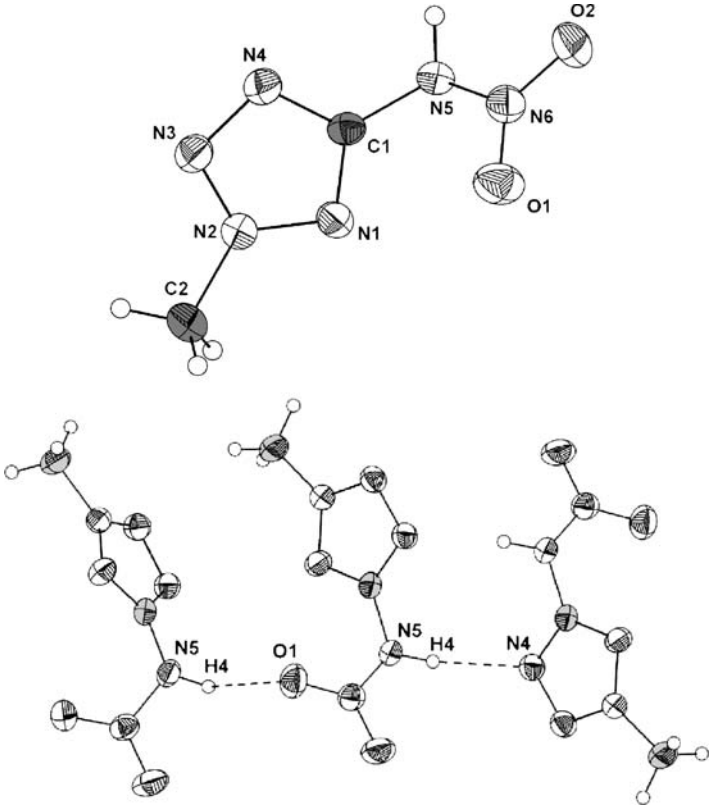

Fig. 23 *Left*: View of the molecular structure of **6**. Thermal ellipsoid are drawn at the 50% probability level and hydrogen atoms are shown as small spheres of arbitrary radii. *Right*: H-bonding in **6** (N5 – H1 – N4^{i}: D – H 0.86(2) Å, H – A 2.13(2) Å, D – A 2.965(2) Å, D – H – A 163 (2)°; N5 – H1 – O1^{ii}: 0,86(2), 2.66(2), 3.070(2), 111.0(18) ((i) – *x*, – *y*, 2 – *z*; (ii) *x*, 0.5 – *y*, 0.5 + *z*))

The ^{13}C and ^{15}N NMR chemical shifts and the $^{15}N - {}^{1}H$ coupling constants are presented in Table 8. For all compounds the proton coupled as well as the proton decoupled ^{15}N NMR spectra (with full NOE) were recorded. The assignments are given based on the values of the $^{15}N - {}^{1}H$ coupling constants and on comparison with the literature [55]. The chemical shifts are given with respect to CH_3NO_2 (^{15}N) and TMS (^{13}C) as external standards. In the case of ^{15}N NMR, negative shifts are upfield from CH_3NO_2. In all cases d_6-DMSO was used as the solvent.

DSC measurements to determine the decomposition temperatures of **2**, **5**, and **6** were performed in covered Al-containers with a nitrogen flow of 20 mL min^{-1} on a PerkinElmer Pyris 6 DSC [83], calibrated by standard pure indium and zinc at a heating rate of 5 °C min^{-1}. The DSC plots in Fig. 25 show the thermal behavior of 1.0 mg of **2**, **5**, and **6** in the 50–300 °C tem-

Table 7 Bond angles of **2**, **5**, and **6**

Atoms	Bond angles (1–2–3) [°]		
	2	**5**	**6**
N2 – N1 – C1	109.87(9)	110.4(1)	101.0(1)
C1 – N4 – N3	110.5(1)	110.2(1)	105.8(1)
N1 – N2 – N3	107.97(9)	107.8(1)	114.1(1)
N6 – N5 – C1	115.43(9)	115.7(1)	117.9(1)
N2 – N3 – N4	107.73(9)	107.7(1)	106.0(1)
N1 – N2 – C2		122.0(1)	
C1 – N1 – C2		127.3(1)	
N2 – N3 – C2			122.1(1)
N1 – N2 – C2			123.8(1)
O1 – N6 – O2	123.5(1)	121.6(1)	126.1(2)
O1 – N6 – N5	122.07(9)	121.9(1)	118.2(1)
O2 – N6 – N5	114.44(9)	116.5(1)	115.6(2)
N4 – C1 – N1	103.9(1)	103.9(1)	113.2(2)
N4 – C1 – N5	121.4(1)	136.9(1)	122.3(1)
N1 – C1 – N5	134.6(1)	119.2(1)	124.5(2)

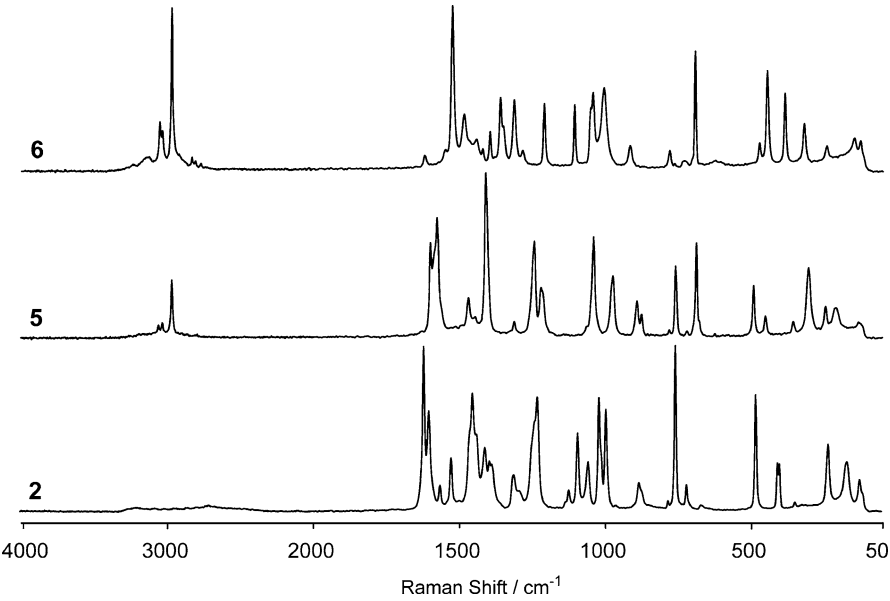

Fig. 24 Solid state Raman spectra of compounds **2** (*bottom*), **5** (*middle*), and **6** (*top*)

perature range. Compound **2** shows the lowest decomposition point at 122 °C, whereby compounds **5** and **6** decompose during melting at 125 °C and 123 °C, as shown by the curve of Fig. 5.

Table 8 ^{15}N NMR and ^{13}C NMR chemical shifts and $^{15}N-^{1}H$ coupling constants

Compound	NMR chemical shift [ppm]						
	δ(N1)	δ(N2)	δ(N3)	δ(N4)	δ(N4)	δ(N6)	δ(C1)
2	– 144.6	– 24.6	– 24.6	– 144.6	– 174.9	– 24.6	152.6
5	– 177.4[a]	– 26.8[b]	– 29.8	– 159.2	– 159.3	– 18.8	150.3
6	– 83.4[b]	– 103.6[c]	– 0.3[b]	– 58.3	– 209.3	– 35.0	157.6

[a] $^{2}J_{N-H}$ =2.1 Hz
[b] $^{3}J_{N-H}$ =1.9 Hz
[c] $^{2}J_{N-H}$ =2.2 Hz

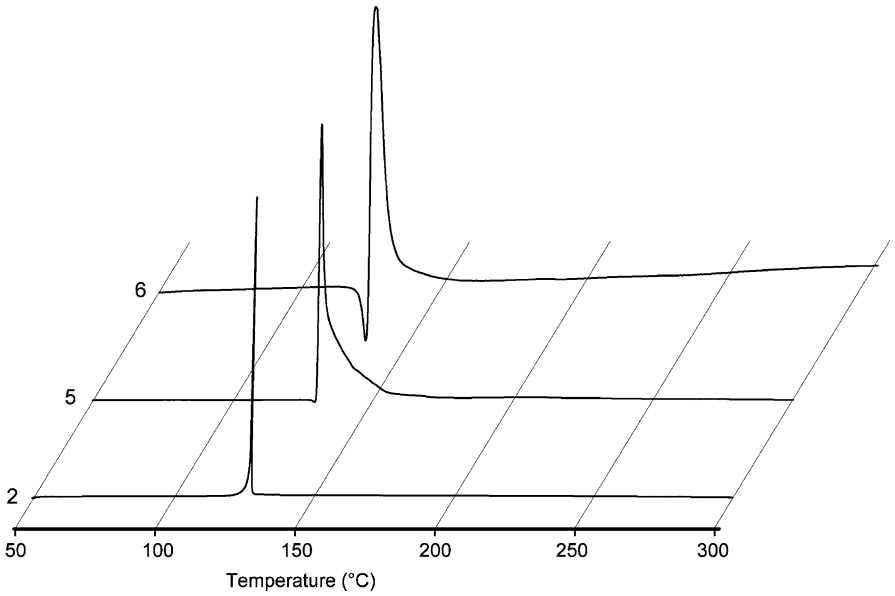

Fig. 25 DSC plot (endo up) of compounds **2**, **5**, and **6** (5 °C min^{-1}). T_{onset}: **2** 122 °C; **5** 125 °C; **6** 123 °C

To determine the heats of decomposition, a Linseis DSC PT10 [84] was used. Three samples (ca. 1 mg) were heated with a heating rate of 2 °C min^{-1} and a fixed nitrogen flow of 5 L h^{-1} over the decomposition peaks. The surface was integrated using the Linseis software and the average of three measurements was calculated to yield heats of decomposition $\Delta_{dec}H^{\circ}_{m}$ of 2638 J g^{-1} (**2**), 1685 J g^{-1} (**5**), and 2158 J g^{-1} (**6**).

For initial safety testing, the impact and friction sensitivities were tested according to BAM methods [85, 86] with the "BAM Fallhammer" and "BAM friction tester". Compound **2** is very sensitive towards impact (< 1.5 J) and

friction (< 8 N) and since the value is comparable with lead azide, it should be considered to be a primary explosive, and should therefore only be handled with appropriate precautions. Compound **5** is moderately sensitive towards impact (< 12.5 J) and friction (< 160 N). However, **6** shows increased sensitivities comparing to **5** (impact: < 3.0 J, friction: < 145 N). Accordingly, **5** and **6** fall into the group of compounds described as "sensitive".

The heats of combustion for the compounds **2**, **5**, and **6** were determined experimentally, using a Parr 1356 bomb calorimeter (static jacket) equipped with a Parr 1108CL oxygen bomb [87]. To ensure better combustion, the samples (ca. 200 mg) were pressed with a defined amount of benzoic acid (ca. 800 mg) to form a tablet and a Parr 45C10 alloy fuse wire was used for ignition. In all measurements, a correction of 2.3 cal cm^{-1} wire burned has been applied, and the bomb was examined for evidence of noncombusted carbon after each run. A Parr 1755 printer was furnished with the Parr 1356 calorimeter to produce a permanent record of all activities within the calorimeter. The reported values are the average of three separate measurements. The calorimeter was calibrated by combustion of certified benzoic acid (SRM, 39i, NIST) in an oxygen atmosphere at a pressure of 3.05 MPa. The experimental results of the constant volume combustion energy ($\Delta_c U$) of the salts are summarized in Table 9. The standard molar enthalpy of combustion ($\Delta_c H°$) was derived from $\Delta_c H° = \Delta_c U + \Delta nRT$ ($\Delta n = \Delta n_i$(products, g) – Δn_i(reactants, g);Δn_i is the total molar amount of gases in the products or reactants). The enthalpy of formation, $\Delta_f H°$, for each of the salts was calculated at 298.15 K using Hess' law and the following combustion reactions:

2: $$CH_2N_6O_2 + 1/2O_2 \rightarrow CO_2 + H_2O + 3N_2 \quad (1)$$

5,6: $$C_2H_4N_6O_2 + 2O_2 \rightarrow 2CO_2 + 2H_2O + 3N_2\,. \quad (2)$$

Table 9 shows that **2**, **5**, and **6** are strongly endothermic compounds ($\Delta_f H°$ **2**: + 264 kJ mol^{-1}, **5**: + 260 kJ mol^{-1}, **6**: + 380 kJ mol^{-1}). The enthalpies of energetic materials are governed by the molecular structure of the compounds, and therefore, heterocycles with a higher nitrogen content (e.g., imidazole $\Delta_f H°_{cryst}$ = 14.0 kcal mol^{-1} [88]; 1,2,4-triazole $\Delta_f H°_{cryst}$ = 26.1 kcal mol^{-1}; tetrazole $\Delta_f H°_{cryst}$ = 56.7 kcal mol^{-1} [89, 90]) show higher heats of formation. From the experimentally determined heats of formation and densities obtained from single crystal structure X-ray diffraction, various thermochemical properties have been calculated using the EXPLO5 software and are summarized in Table 9.

The detonation parameters were calculated using the program EXPLO5 V5.02 [91, 92] and are summarized in Table 9. The program is based on the steady-state model of equilibrium detonation and uses BKW E.O.S [93] for gaseous detonation products and Cowan–Fickett E.O.S. for solid carbon. The calculations were performed using the maximum densities according to the crystal structures and the BKWN set of constants was used. **2** shows a very

Table 9 Physico-chemical properties of **2**, **5**, and **6**

	2	**5**	**6**
Formula	$CH_2N_6O_2$	$C_2H_4N_6O_2$	$C_2H_4N_6O_2$
Molecular mass	130.09	144.11	144.11
Impact sensitivity [J][a]	1.5	12.5	3.0
Friction sensitivity [N][b]	8	160	145
Electrical discharge	No reaction	No reaction	No reaction
N [%][c]	64.61	58.32	58.32
Ω [%][d]	– 12.30	– 44.41	– 44.41
Combustion	Yes	Yes	Yes
T_{dec} [°C][e]	122	125	122
Density [g cm^{-3}][f]	1.87	1.76	1.67
$-\Delta_c U$ [cal g^{-1}][g]	1750	2700	2902
$-\Delta_c H°$ [kJ mol^{-1}][h]	944	1619	1740
$\Delta_f H_m^\circ$ [kJ mol^{-1}][i]	264	260	380
$\Delta_{dec} H_m^\circ$ [J g^{-1}][j]	2638	1685	2158
$-\Delta_E U_m^\circ$ [J g^{-1}][k]	5326	5235	5998
T_E [K][l]	4309	3824	4283
P [kbar][m]	363	295	289
D [m s^{-1}][n]	9173	8433	8434
Gas volume [mL g^{-1}][o]	404	395	413

[a] BAM methods, insensitive > 40 J, less sensitive ≥ 35 J, sensitive ≥ 4 J, very sensitive ≤ 3 J [85, 86];
[b] BAM methods, insensitive > 360 N, less sensitive = 360 N, sensitive < 360 N to > 80 N, very sensitive ≤ 80 N, extremely sensitive ≤ 10 N [85, 86];
[c] Nitrogen content;
[d] Oxygen balance;
[e] Decomposition temperature from DSC (β = 5 °C);
[f] Estimated from X-ray diffraction;
[g] Experimental (constant volume) combustion energy;
[h] Experimental molar enthalpy of combustion;
[i] Molar enthalpy of formation;
[j] Experimental enthalpy of decomposition using DSC;
[k] Energy of explosion, EXPLO5 V5.02;
[l] Explosion temperature, EXPLO5 V5.02;
[m] Detonation pressure, EXPLO5 V5.02;
[n] Detonation velocity, EXPLO5 V5.02;
[o] Assuming only gaseous products, EXPLO5 V5.02

high calculated detonation pressure of 363 kbar and a detonation velocity of 9173 m s^{-1} higher than TNT (P = 202 kbar, D = 7150 m s^{-1}) [91]. Even compound **5** also shows promising values for the detonation pressures (295 kbar) and explosion velocity (8433 m s^{-1}). The influence of the density on the properties of energetic materials is clearly shown by **6**, which shows the lowest

detonation pressure of 289 kbar in spite of the highest positive heat of formation due to its low density.

In order to determine the thermal decomposition products, the compounds were heated in a evacuated steel tube for ca. 30 s at a temperature of 250 °C and the gaseous products were transferred into an evacuated gas IR cell. Figure Fig. 26 shows the gas phase IR spectra of the decomposition products of **2**, **5**, and **6**.

The thermal decomposition of **2** results in the formation of only two main products, which could be identified using IR spectroscopy, namely CO_2 [94] and CO [95]. In addition trace amounts of HCN and CH_4 were visible in the gas-phase IR spectrum, however, no evidence for the formation of water vapor was found. In the methylated compounds, many more decomposition products were observed using gas-phase IR spectroscopy. Besides CO_2 and CO, larger amounts of CH_4 [96] and HCN were found in the decomposition of **5** and **6**, in comparison with **2**. In contrast to **5**, where bigger amounts of expected NH_3 were detected, the thermal decomposition of **6** shows only traces of NH_3 but moderate amounts of N_2O [97].

The electrostatic potentials were illustrated after computing a optimal geometry at the B3LYP/6-31G* level of theory using the program package HyperChem 7.52 [98]. Figure 27 shows the 0.001 electron bohr^{-3} 3D isosurface of electron density for **2**, **5**, and **6**. In these diagrams a Jorgensen–Salem

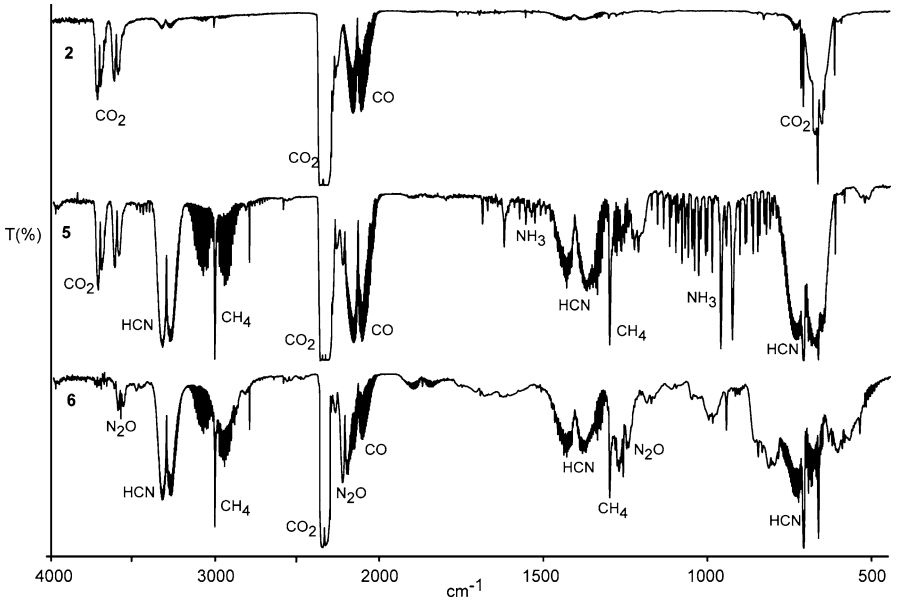

Fig. 26 IR spectra showing the gas-phase decomposition products of **2** (*top*), **5** (*middle*), and **6** (*bottom*)

Fig. 27 Calculated (B3LYP /6-31G*) electrostatic potential of **2** (*left*), **5** (*middle*), and **6** (*right*). The *dark regions* represent electron-rich regions, the *light regions* electron-deficient regions

representation was chosen with an electrostatic potential contour value of 0.07 hartree. The dark regions represent extremely electron-rich regions (V(r) < 0.07 hartree) and the light regions extremely electron-deficient regions (V(r) > 0.071 hartree). In general, the patterns of the calculated electrostatic potentials of the surface of molecules can be related to the impact sensitivities [99–106]. In contrast to non-energetic organic molecules where the positive potential is larger but weaker in strength, in nitro and azo compounds usually more extensive regions with larger and stronger positive potentials are observed, which can be related to the increased impact sensitivities.

Long-term stability tests were performed using a Systag FlexyTSC [107] (thermal safety calorimetry) in combination with a RADEX V5 oven and the SysGraph software. The tests were undertaken as long-term isoperibolic evaluations in glass test vessels at atmospheric pressure with ca. 200 mg of the compounds. It was shown that tempering a substance for 48 h at 40 °C under the decomposition point results in a storage period of 58 years at room temperature. In our cases we chose a temperature of 80 °C and investigated the possible occurrence of exo- or endothermic behavior over a period of 48 h (Fig. 28). **2** and **5** were completely stable for 48 h, while **6** showed negligible minimal exothermic steps in the first 6 h. It can therefore be reasoned, that all

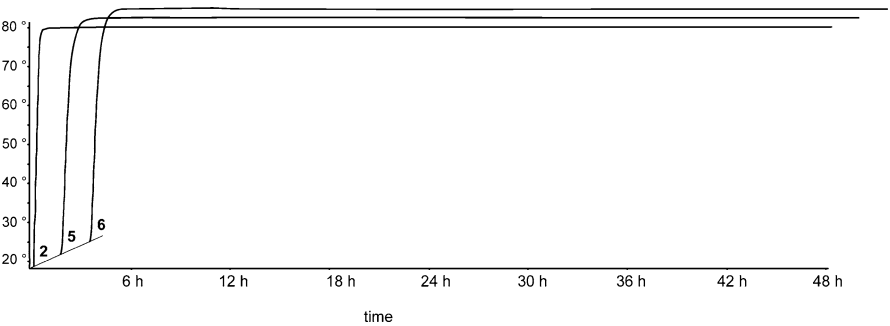

Fig. 28 Long-term stability screen of **2**, **5**, and **6** using a FlexyTSC (80 °C, 48 h)

three compounds show long-term stability, which is a basic requirement for possible applications.

From the combined experimental and computational study discussed in this chapter the following conclusions can be drawn:

- 5-Nitriminotetrazole (**2**), 1-methyl-5-nitriminotetrazole (**5**), and 2-methyl-5-nitraminotetrazole (**6**) can be synthesized in high yields and purity from aminotetrazole and 1- and 2-methyl-5-aminotetrazole, respectively, in simple one-step syntheses by reaction with fuming HNO_3.
- The crystal structures of **2**, **5**, **6** were determined using low-temperature single crystal X-ray diffraction. In the structure of **2** both hydrogen atoms could be located at the tetrazole ring forming a nitriminotetrazole. A similar structure can be observed for **5**, whereas **6** corresponds to a nitraminotetrazole, where the hydrogen atom is located at the nitrogen atom of the nitramine group. All of the compounds are stabilized in the crystalline state because of the presence of strong hydrogen bonds.
- Thorough characterization of the chemical, thermochemical, and energetic properties of **2**, **5** and **6** is reported. All compounds presented are energetic materials, showing increased sensitivities towards friction and impact and have long-term stability at room temperature. In the case of **2**, increased precautions should be undertaken when the compound is prepared on a larger scale.

3.5 1,6-Dimethyl-5-nitraminotetrazole

In an early publication [108] our research group inadvertently published a wrong value for the heat of formation determined from bomb-calorimetric measurements.

In the publication we described several nitroso- and nitraminotetrazoles, including 1,6-dimethyl-5-nitraminotetrazole (Fig. 29), as products of the nitration of 1,6-dimethyl-5-aminotetrazole using a mixture of nitric acid (100%) and trifluoroacetic anhydride (Fig. 30).

In the thermochemistry part of the earlier publication [108] a heat of formation of + 2.8 kcal mol^{-1} was reported. According to recent calculations by Rice et al. (see chapter in this volume), however, the heat of forma-

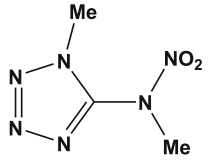

$C_3H_6N_6O_2$

Mol. Wt.: 158,12

C, 22.79; H, 3.82;
N, 53.15; O, 20.24

Fig. 29 1,6-Dimethyl-5-nitraminotetrazole

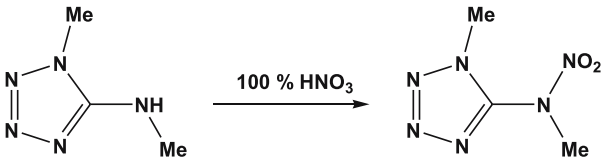

Fig. 30 Synthesis of 1,6-dimethyl-5-nitraminotetrazole

tion was expected to be 70 kcal mol^{-1}. This prompted us to synthesize 1,6-dimethyl-5-nitraminotetrazole again and to re-investigate the heat of combustion (Table 10). From the re-determined experimental heat of combustion of 564 kcal mol^{-1}, a heat of formation of 75 kcal mol^{-1} was then calculated, which is in much better agreement with the predicted value of 70 kcal mol^{-1}.

The calorimetric measurements were performed using a Parr 1356 bomb calorimeter (static jacket) equipped with a Parr 1108CL oxygen bomb for the combustion of highly energetic materials [87]. The samples (ca. 200 mg) were pressed with a well-defined amount of benzoic acid (ca. 800 mg) forming a tablet and a Parr 45C10 alloy fuse wire was used for ignition. In all measurements a correction of 2.3 (IT) cal cm^{-1} wire burned has been applied, and the bomb was examined for evidence of noncombusted carbon after each run. A Parr 1755 printer was furnished with the Parr 1356 calorimeter to produce a permanent record of all activities within the calorimeter. The reported values are the average of three single measurements. The calorimeter was calibrated by combustion of certified benzoic acid (SRM, 39i, NIST) in an oxygen atmosphere at a pressure of 3.05 MPa. The standard molar enthalpy of combustion ($\Delta_c H°$) was derived from $\Delta_c H° = \Delta_c U + \Delta nRT$ ($\Delta n = \Delta n_i$(products, g) – Δn_i(reactants, g); Δn_i is the total molar amount of gases in the products or reactants). The enthalpy of formation, $\Delta_f H°$, for each of the salts was calculated at 298.15 K using the Hess' law and the following combustion reaction:

$$C_3H_6N_6O_2 + 3.5O_2 \rightarrow 3CO_2(g) + 3H_2O(l) + 3N_2(g) \quad \Delta n = 2.5\,.$$

The heats of formation of the combustion products were obtained from the literature (NIST) [96].

Table 10 Thermodynamic values of 1,6-dimethyl-5-nitraminotetrazole

	Correct values	Wrong published values
$\Delta_c U$ [cal g^{-1}]	3565	3119
$\Delta_c U$ [kcal mol^{-1}]	564	490
$\Delta_f H°$ [kcal mol^{-1}]	75	2.8
Calculated $\Delta_f H°$	70	

4
Neutral Nitramine Compounds

4.1
Dinitrobiuret (DNB)

The LMU Munich research group has also been looking at tetrazole-free nitrogen-rich compounds that contain oxidizing groups such as nitramine functionalities. In this context, the preparation and structural characterization of dinitrobiuret (DNB) (Fig. 31) was carried out [109, 110]. The high chemical and thermal stability of DNB and the determined critical diameter of 6 mm for DNB (Figs. 32, 33) in the Koenen test (steel shell test) is comparable to the values reported for HMX (8 mm), RDX (8 mm), or PETN (6 mm) and prompted us to obtain the thermodynamic data and detonation pressures and velocities for DNB in a combined experimental and theoretical study.

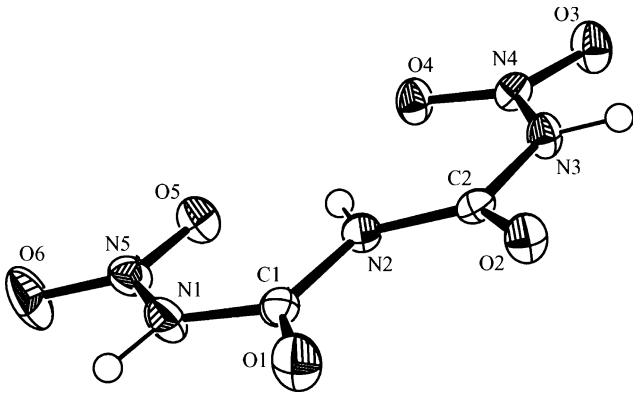

Fig. 31 Molecular structure of DNB in the crystalline state

The heat of combustion ($\Delta_c H$) of dinitrobiuret (DNB) was determined experimentally using oxygen bomb calorimetry: $\Delta_c H(\text{DNB}) = 5195 \pm 200\ \text{kJ kg}^{-1}$. The standard heat of formation ($\Delta_f H°$) of DNB was obtained on the basis of quantum chemical computations at the electron-correlated ab initio MP2 (second order Møller–Plesset perturbation theory) level of theory using a correlation consistent double-zeta basis set (cc-pV-DZ): $\Delta_f H°(\text{DNB}) = -353\ \text{kJ mol}^{-1}$, $-1829\ \text{kJ kg}^{-1}$ (Fig. 34). The detonation velocity (D) and detonation pressure (P) of DNB was calculated using the empirical equations by Kamlet and Jacobs: $D(\text{DNB}) = 8.66\ \text{mm}\ \mu\text{s}^{-1}$, $P(\text{DNB}) = 33.9$ GPa.

From this combined experimental and theoretical study the following conclusions could be drawn:

1. Dinitrobiuret (DNB) is a very powerful and promising new explosive

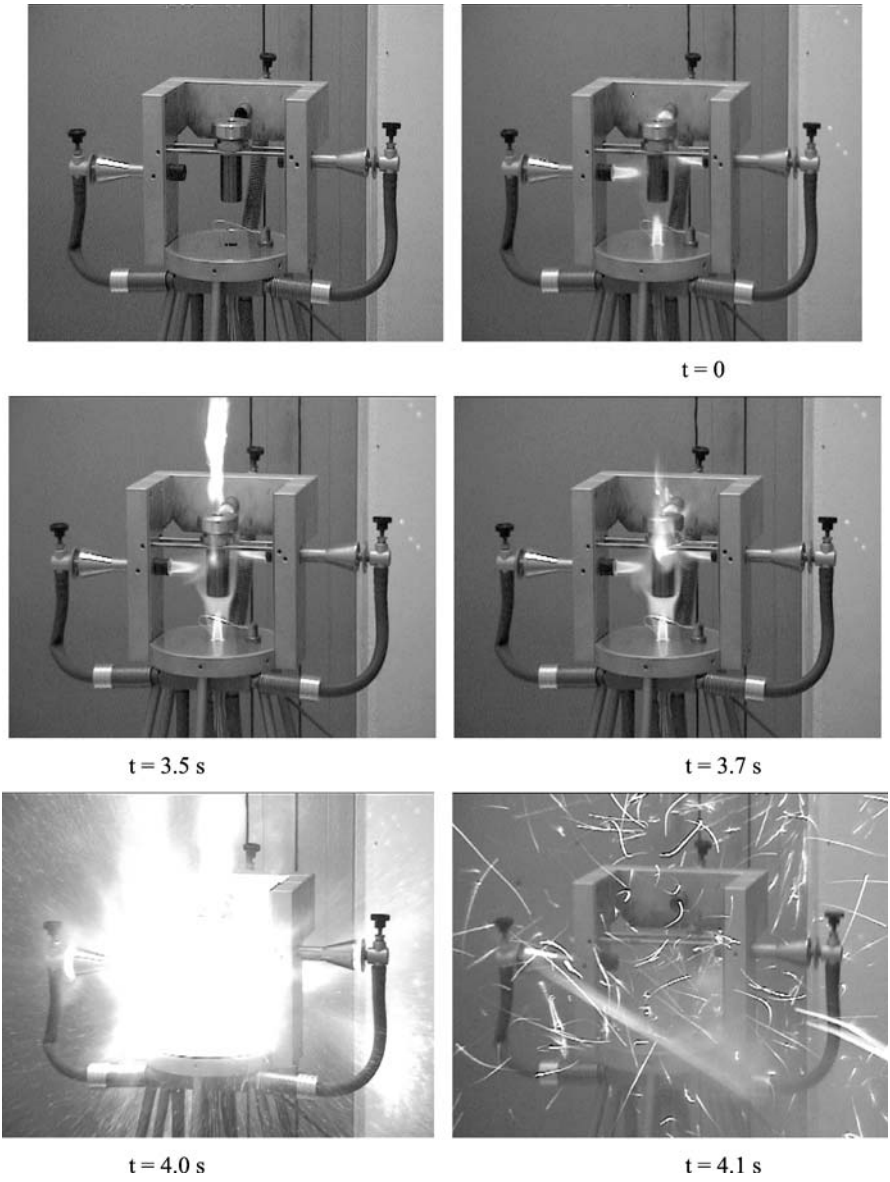

Fig. 32 Steel sleeve test of DNB (10 g, 6 mm)

2. DNB has an almost neutral, even slightly positive oxygen balance of + 4.1%
3. DNB shows a detonation velocity and detonation pressure similar to well-established energetic materials such as PETN, RDX, or HMX

Fig. 33 Steel sleeve test of DNB (10 g, 6 mm) before (*left*) and after test (*right*)

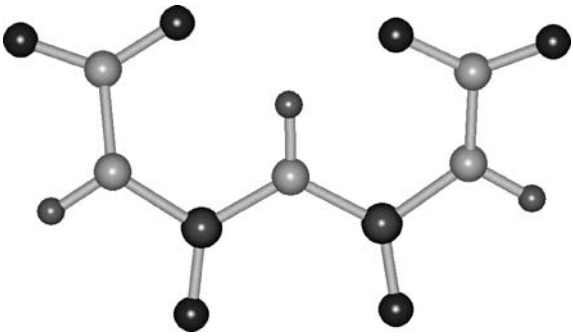

Fig. 34 Ab initio (MP2/cc-pVDZ) computed molecular structure of DNB

Acknowledgements Financial support of this work by the University of Munich (LMU), the Fonds der Chemischen Industrie (FCI) and the European Research Office (ERO) of the US Army Research Laboratory (ARL) under contract nos. 9939-AN-01 & N 62558-

05-C-0027 and the Bundeswehr Research Institute for Materials, Explosives, Fuels and Lubricants (WIWEB) under contract nos. E/E210/4D004/X5143 and E/E210/7D002/4F088 is gratefully acknowledged. The work presented in this chapter would not have been possible without the help of several outstanding coworkers in the LMU research group. The author especially thanks Prof. Konstantin Karaghiosoff, Dr. habil. Margaret-Jane Crawford, Dr. Jan J. Weigand, Dipl.-Chem. Michael Göbel and Dipl.-Chem. Jörg Stierstorfer for their help and support. Ms. Carmen Nowak is thanked for drawing all structures and preparing the figures and Ms. Irene Scheckenbach for her help with a difficult manuscript.

References

1. Klapötke TM, Holl G (2001) Green Chem 3:G75
2. Klapötke TM, Holl G (2002) Chem Aust, p 11
3. Kanekar P, Dautpure P, Sarnaik S (2003) Ind J Exp Biol 41:991
4. Robidoux PY, Gong P, Sarrazin M, Bardai G, Paquet L, Hawari J, Dubois C, Sunahara GI (2004) Can Ecotoxicol Environ Safe 58:300
5. Robidoux PY, Sunahara GI, Savard K, Berthelot Y, Dodard S, Martel M, Gong P, Hawari J (2004) Can Environ Toxicol Chem 23:1026
6. Simini M, Checkai RT, Kuperman RG, Phillips CT, Kolakowski JE, Kurnas CW, Sunahara GI (2003) Pedobiologia 47:657
7. Robidoux PY, Hawari J, Bardai G, Paquet L, Ampleman G, Thiboutot S, Sunahara GI (2002) Can Arch Environ Contam Toxicol 43:379
8. Steevens JA, Duke BM, Lotufo GR, Bridges TS (2002) Environ Toxicol Chem 21:1475
9. Pennington JC, Brannon JM (2002) Thermochim Act 384:163
10. Fournier D, Halasz A, Spain J, Spanggord RJ, Bottaro JC, Hawari J (2004) Appl Environment Microbiol 70:1123
11. Doherty RM (2003) In: De Luca LT, Galfetti L, Pesce-Rodriguez RA (eds) Novel energetic materials and applications. Proceedings of the 9th IWCP, Lerici, La Specia, Italy
12. Karaghiosoff K, Klapötke TM, Michailovski A, Nöth H, Suter M (2003) Prop Explos Pyrotech 28:1
13. Klapötke TM, Krumm B, Holl G, Kaiser M (1999) Proc of 30th int annual conference of ICT, June 29–July 2, Karlsruhe, Germany, p 120
14. Hammerl A, Klapötke TM, Nöth H, Warchhold M, Holl M, Kaiser M (2001) Inorg Chem 40:3570
15. Klapötke TM (2007) Nichtmetallchemie. In: Riedel E (ed) Moderne Anorganische Chemie, 3rd edn. Walter de Gruyter, Berlin
16. Eremets MI, Gavriliuk AG, Serebryanaya NR, Trojan IA, Dzivenko DA, Boehler R, Mao HK, Hemley RJ (2004) J Chem Phys 121:11296
17. Eremets MI, Gavriliuk AG, Trojan IA, Dzivenko DA, Boehler R (2004) Nat Mater 3:558
18. Eremets MI, Popov MY, Trojan IA, Denisov VN, Boehler R, Hemley RJ (2004) J Chem Phys 120:10618
19. Christe KO, Wilson WW, Sheehy JA, Boatz JA (1999) Angew Chem Int Ed 38:2004
20. Vij A, Wilson WW, Vij V, Tham FS, Sheehy JA, Christe KO (2001) J Am Chem Soc 123:6308
21. Klapötke TM (1999) Angew Chem 111:2694
22. Schroer T, Haiges R, Schneider S, Christe KO (2005) Chem Comm, p 1607

23. Vij A, Pavlovich JG, Wilson WW, Vij V, Christe KO (2002) Angew Chem Int Ed 41:3051
24. Lauderdale WJ, Stanton JF, Bartlett RJ (1992) J Phys Chem 96:1173
25. Perera SA, Bartlett RJ (1999) Chem Phys Lett 314:381
26. Tobita M, Bartlett RJ (2001) J Phys Chem A 105:4107
27. Glukhovtsev MN, Jiao H, Schleyer PVR (1996) Inorg Chem 35:7124
28. Glukhovtsev MN, Schleyer PVR (1992) Chem Phys Lett 198:547
29. Klapötke TM (2000) J Mol Struct (THEOCHEM) 499:99
30. Klapötke TM, Harcourt RD (2001) J Mol Struct (THEOCHEM) 541:237
31. Schmidt MW, Gordon MS, Boatz JA (2005) J Phys Chem A 109:7285
32. Wang R, Gao H, Ye C, Twamley B, Shreeve JM (2007) Inorg Chem 46:932
33. Geith J, Klapötke TM, Weigand JJ, Holl H (2004) Prop Explos Pyrotech 29:3
34. Klapötke TM, Mayer P, Schulz A, Weigand JJ (2005) J Am Chem Soc 127:2032
35. Fischer G, Holl G, Klapötke TM, Weigand JJ (2005) Thermochim Acta 437:168
36. Raap R (1969) Can J Chem 47:3677
37. Gaponik PN, Karavai VP (1984) Khim Geterotsikl Soedin 12:1683
38. Stolle R, Netz H, Kramer O, Rothschild S, Erbe E, Schick O (1933) J Prak Chem 138:1
39. Gálvez-Ruiz JC, Holl G, Karaghiosoff K, Klapötke TM, Löhnwitz K, Mayer P, Nöth H, Polborn K, Rohbogner CJ, Suter M, Weigand JJ (2005) Inorg Chem 44:4237
40. Darwich C, Klapötke TM (2006) New trends in research of energetic materials. Proceedings of the 9th seminar, Pardubice, Czech Republic, p 551
41. Gálvez-Ruiz JC, Holl G, Karaghiosoff K, Klapötke TM, Löhnwitz K, Mayer P, Nöth N, Polborn K, Rohbogner CJ, Suter M, Weigand JJ (2005) Inorg Chem 44:5192
42. Boese R, Klapötke TM, Mayer P, Verma V (2006) Prop Explos Pyrotech 31:263
43. Murray WM, Sauer WC (Arthur D, Little Inc) (1961) US Patent 3006957
44. Marans NS, Zelinski RP (1950) J Am Chem Soc 72:5329
45. Göbel M, Klapötke TM (2007) New trends in research of energetic materials. Proceedings of the 10th seminar, Pardubice, Czech Republic, p L13
46. Adam D, Karaghiosoff K, Holl G, Kaiser M, Klapötke TM (2002) Prop Explos Pyrotech 27:7
47. Karaghiosoff K, Klapötke TM, Michailovski A, Nöth H, Suter M (2003) Prop Explos Pyrotech 28:1
48. Klapötke TM, Mayer P, Verma V (2006) Prop Explos Pyrotech 31:263
49. Deal WE (1957) J Chem Phys 27:796
50. Mader CL (1963) Report LA-2900: Fortran BKW code for computing the detonation properties of explosives. Los Alomos Scientific Laboratory, NM
51. Urbanski T (1985) Chemistry and technology of explsoives. Pergamon, England
52. Astakhov AM, Vasilev AD, Molokeev MS, Revenko VA, Stepanov RS (2005) Russ J Org Chem 41:910
53. Klapötke TM, Stierstorfer J (2007) New trends in research of energetic materials. Proceedings of the 10th seminar, Pardubice, Czech Republic, p 35
54. Bryden JH (1953) Acta Cryst 6:669
55. Karahiosoff K, Klapötke TM, Mayer P, Piotrowski H, Polborn K, Willer RL, Weigand JJ (2005) J Org Chem 71:1295
56. Tappan BC, Beal RW, Brill TB (2002) Thermochim Act 288:227
57. Tappan BC, Incarnito CD, Rheingold AL, Brill TB (2002) Thermochim Act 384:113
58. Brill TB, Tappan BC, Beal RW (2001) New trends in research of energetic materials. Proceedings of the 4th seminar, Pardubice, Czech Rep, p 17
59. Thiele J (1892) Ann 270:1
60. Herbst RM, Garrison JA (1953) J Org Chem 18:941

61. Lieber E, Sherman E, Henry RA, Cohen J (1951) J Am Chem Soc 73:2327
62. Astachov AM, Nefedo AA, Vasiliev AD, Kruglyakova LA, Dyugaev KP, Stepanov RS (2005) Proc of 36th int annual conference of ICT, Jun 28–July 1, Karlsruhe, Germany, p 113
63. Lieber E, Sherman E, Henry RA, Cohen J (1951) J Am Chem Soc 73:2327
64. O'Connor TE, Fleming G, Reilly J (1949) J Soc Chem Ind (London) 68:309
65. Mayants AG, Klimenko VS, Erina VV, Pyreseva KG, Gordeichuk SS, Leibzon VN, Kuz'min VS, Burtsev UN (1991) Khim Geterot Soed 8:1067
66. Göbel M, Klapötke TM, Mayer E (2006) Z Anorg Allg Chem 2632:1043
67. Thiele J (1892) Ann 270:1
68. Henry RA, Finnegan WG (1954) J Am Chem Soc 76:923
69. Henry RA, Finnegan WG (1956) J Am Chem Soc 78:411
70. Oxford Diffraction (2005) CrysAlis CCD, Version 1.171.27p5 beta (release 01-04-2005 CrysAlis171.NET)
71. Oxford Diffraction (2005) CrysAlis RED, Version 1.171.27p5 beta (release 01-04-2005 CrysAlis171.NET)
72. Altomare A, Cascarano G, Giacovazzo C, Guagliardi A (1993) SIR-92, A program for crystal structure solution. J App Cryst 26:343
73. Sheldrick GM (1994) SHELXL97 program for the refinement of crystal structures. University of Göttingen, Germany
74. Spek AL (1999) PLATON, a multipurpose crystallographic tool. Utrecht University, Utrecht, The Netherlands
75. Oxford Diffraction (2005) SCALE3 ABSPACK (1.0.4,gui:1.0.3) (C)
76. Cambridge Crystallographic Data Centre (2007) http://www.ccdc.cam.ac.uk/, last visited: 30 Mar 2007
77. Lieber E, Patinkin T (1951) J Am Chem Soc 73:1792
78. Bray DD, White JG (1979) Acta Cryst B 35:3089
79. Riedel E (1999) Anorganische Chemie, 4th edn. Walter de Gruyter, Berlin, p 134
80. Lieber E, Levering DR, Patterson LJ (1951) Anal Chem 23:1594
81. Weigand JJ (2005) Dissertation, Ludwig Maximilian University Munich
82. Daszkiewicz Z, Nowakowska EM, Preźdo WW, Kyzioł JB (1995) Pol J Chem 69:1437
83. PerkinElmer (2007) http://www.perkinelmer.com, last visited: 30 Mar 2007
84. Linseis (2007) http://www.linseis.com, last visited: 30 Mar 2007
85. United Nations Economic Commission for Europe (2005) UN recommendations on the transport of dangerous goods, 14th edn. http://www.unece.org/trans/danger/publi/unrec/rev14/14files_.html, last visited: 30 Mar 2007
86. Bundesanstalt für Materialforschung und -prüfung (2007) http://www.bam.de, last visited: 30 Mar 2007
87. Parr Instrument Company (2007) http://www.parrinst.com, last visited: 30 Mar 2007
88. West RC, Selby SM (eds) (1967–1968) Handbook of chemistry and physics, 48th edn. CRC, Cleveland, OH
89. McEwan WS, Rigg MW (1951) J Am Chem Soc 73:4725
90. Ostrovskii VA, Pevzner MS, Kofman TP, Tselinskii IV (1999) Targets Heterocycl Syst 3:467
91. Suceska M (1999) Proc of 30th int annual conference of ICT, June 29–July 2, Karlsruhe, Germany, p 50
92. Suceska M (2001) EXPLO5.V2: computer program for calculation of detonation parameters. Proc of 32nd int annual conference of ICT, July 3–6, Karlsruhe, German, p 110
93. Suceska M (1991) Prop Explos Pyrotech 16:197

94. Mecke R, Langenbucher F (1965) Infrared spectra. Heyden, London, Serial no. 6
95. Shimanouchi T (1972) Tables of molecular vibrational frequencies consolidated, vol II. J Phys Chem Ref Data 6:993
96. National Institue of Standards and Technology (2007) Vibrational energy search http://webbook.nist.gov/chemistry/vib-ser.html, last visited: 30 Mar 2007
97. Nakamoto K (1986) Infrared and Raman Spectra of inorganic and coordination compounds, 4th edn. Wiley, New York
98. Hypercube (2002) HyperChem 7.52: Molecular visualization and simulation program package. Hypercube, Gainsville, FL
99. Murray JS, Lane P, Politzer P (1995) Mol Phys 85:1
100. Murray JS, Lane P, Politzer P (1998) Mol Phys 93:187
101. Politzer P, Murray JS (1999) Computational characterization of energetic materials. In: Maksic ZB, Orville-Thomas WJ (eds) Pauling's legacy: modern modelling of the chemical bond. Theor Comput Chem 6:347
102. Politzer P, Murray JS, Seminario JM, Lane P, Grice ME, Concha MC (2001) J Mol Struct (THEOCHEM) 573:1
103. Rice BM, Chabalowski CF, Adams GF, Mowrey RC, Page M (1991) Chem Phys Lett 184:335
104. Rice BM, Hare JJ (2002) J Phys Chem A 106:1770
105. Rice BM, Sahu S, Owens FJ (2002) J Mol Struct (THEOCHEM) 583:69
106. Rice BM (2005) Adv Ser Phys Chem 16:33
107. Systag (2007) Process development and safety http://www.systag.ch, last visited: 30 Mar 2007
108. Karaghiosoff K, Klapötke TM, Mayer P, Piotrowski H, Polborn K, Willer RL, Weigand JJ (2005) J Org Chem 71:1295
109. Geith J, Klapötke TM, Weigand JJ, Holl G (2004) Prop Explos Pyrotech 29:3
110. Geith J, Holl G, Klapötke TM, Weigand JJ (2004) Combust Flame 139:358